Plant, Cell & Environment

Plant, Cell and Environment (2015) **38**, 1200–1211 doi: 10.1111/pce.12459

Technical Report

Partitioning changes in photosynthetic rate into contributions from different variables

Thomas N. Buckley[1] & Antonio Diaz-Espejo[2]

[1]IA Watson Grains Research Centre, Faculty of Agriculture and Environment, University of Sydney, Narrabri, NSW 2390, Australia and [2]Irrigation and Crop Ecophysiology Group, Instituto de Recursos Naturales y Agrobiología de Sevilla (IRNAS, CSIC), Sevilla 41012, Spain

ABSTRACT

Changes in net CO_2 assimilation rate (A) are often partitioned into contributions from changes in different variables using an approach that is based on an expression from calculus: namely the definition of the exact differential of A, which states that an infinitesimal change in A (dA) is equal to the sum of infinitesimal changes in each of the underlying variables, each multiplied by the partial derivative of A with respect to the variable. Finite changes in A can thus be partitioned by integrating this sum across a finite interval. The most widely used method of estimating that integral is a coarse discrete approximation that uses partial derivatives of the natural logarithm of A rather than A itself. This yields biased and ambiguous estimates of partitioned changes in A. We present an alternative partitioning approach based on direct numerical integration of dA. The new approach does not require any partial derivatives to be computed, and it can be applied under any conditions to estimate the contributions from changes in any photosynthetic variable. We demonstrate this approach using field measurements of both seasonal and diurnal changes in assimilation rate, and we provide a spreadsheet implementing the new approach.

Key-words: mesophyll conductance; non-stomatal limitation; photosynthesis; quantitative limitations analysis; stomatal conductance; stomatal limitation; V_{cmax}.

INTRODUCTION

It is often useful to quantify the impact of changes in various factors on net CO_2 assimilation rate (A). Jones (1985) proposed an approach in which a finite change in A is partitioned into percentage contributions from changes in several underlying variables. This approach was later modified by Wilson *et al*. (2000) and then extended by Grassi & Magnani (2005), and the version proposed by the latter authors (hereafter the 'GM' approach) has been widely adopted in recent years (e.g. Flexas *et al*. 2006a,b, 2009, 2014; Galmés *et al*. 2007; Niinemets 2007; Galle *et al*. 2009, 2011; Perez-Martin *et al*. 2009, 2014; Keenan *et al*. 2010a,b; Limousin *et al*. 2010; Misson *et al*. 2010; Sagardoy *et al*. 2010; Egea *et al*. 2011; Tomás *et al*. 2013).

The GM approach is based on the definition of the total differential of a multivariate function. That definition states that an infinitesimal change in a function equals the sum of infinitesimal changes in the function's variables, each multiplied by the function's partial derivative with respect to that variable. For example, if A is expressed as a function of N variables (x_j, where $j = 1$ to N), then the total differential of A (dA) is

$$dA = \frac{\partial A}{\partial x_1}dx_1 + \frac{\partial A}{\partial x_2}dx_2 + \cdots + \frac{\partial A}{\partial x_N}dx_N = \sum_{j=1}^{N}\frac{\partial A}{\partial x_j}dx_j, \quad (1)$$

where dx_j is an infinitesimal change in x_j (Table 1 lists symbols with descriptions and units). Integrating Eqn 1 across a finite interval would thus partition the finite change in A across that interval into components due to the variables x_j. The GM approach applies Eqn 1 to light-saturated assimilation rate (A_{max}), with stomatal conductance to CO_2 (g_{sc}), mesophyll conductance (g_m) and carboxylation capacity (V_{cmax}) treated as variables:

$$dA_{max} = \left(\frac{\partial A_{max}}{\partial g_{sc}}\right)dg_{sc} + \left(\frac{\partial A_{max}}{\partial g_m}\right)dg_m + \left(\frac{\partial A_{max}}{\partial V_{cmax}}\right)dV_{cmax}. \quad (2)$$

This expression is divided by A_{max} to express the changes in relative terms:

$$\frac{dA_{max}}{A_{max}} = \left(\frac{\partial \ln A_{max}}{\partial \ln g_{sc}}\right)\frac{dg_{sc}}{g_{sc}} + \left(\frac{\partial \ln A_{max}}{\partial \ln g_m}\right)\frac{dg_m}{g_m} + \left(\frac{\partial \ln A_{max}}{\partial \ln V_{cmax}}\right)\frac{dV_{cmax}}{V_{cmax}}$$
$$\equiv l_s\frac{dg_{sc}}{g_{sc}} + l_{mc}\frac{dg_m}{g_m} + l_b\frac{dV_{cmax}}{V_{cmax}}. \quad (3)$$

The partial derivatives in Eqn 3 (l_s, l_{mc} and l_b) are functions of g_{sc}, g_m, V_{cmax} and other photosynthetic parameters. To apply Eqn 3 to finite changes in A_{max}, g_{sc}, g_m and V_{cmax}, the GM approach approximates the differentials in Eqn 3 with finite differences between two measurement points (called the 'reference' and 'comparison' points, respectively), then computes each partial derivative at both points and uses the average of the resulting two values:

Correspondence: T. N. Buckley. e-mail: t.buckley@sydney.edu.au

Table 1. List of mathematical symbols including units

Description	Symbol	Units
Net CO_2 assimilation rate (reference value)	A (A_{ref})	μmol m^{-2} s^{-1}
Light-saturated net CO_2 assimilation rate (reference value)	A_{max} ($A_{max,R}$)	μmol m^{-2} s^{-1}
A expressed as a function of 25 °C values and T	A_{25T}	μmol m^{-2} s^{-1}
Ambient CO_2 mole fraction	c_a	μmol mol^{-1}
Intercellular CO_2 mole fraction	c_i	μmol mol^{-1}
Infinitesimal change in A (in A_{max})	dA (dA_{max})	μmol m^{-2} s^{-1}
Finite change in A (in A_{max})	δA (δA_{max})	μmol m^{-2} s^{-1}
Finite change in x_j	δx_j	varies
Initial slope of response of J to i (at 25 °C)	ϕ (ϕ_{25})	dimensionless
Total conductance to CO_2	g	mol m^{-2} s^{-1}
Boundary layer conductance to CO_2	g_{bc}	mol m^{-2} s^{-1}
Mesophyll conductance to CO_2 (at 25 °C)	g_m (g_{m25})	mol m^{-2} s^{-1}
Value of g_m at reference point (at comparison point)	$g_{m,R}$ ($g_{m,C}$)	mol m^{-2} s^{-1}
Stomatal conductance to CO_2	g_{sc}	mol m^{-2} s^{-1}
Value of g_{sc} at reference point (at comparison point)	$g_{sc,R}$ ($g_{sc,C}$)	mol m^{-2} s^{-1}
Photorespiratory CO_2 compensation point (at 25 °C)	Γ_* (Γ_{*25})	μmol mol^{-1}
Photosynthetic photon flux	i	μmol m^{-2} s^{-1}
Index of arbitrary variable that affects A	j	–
Potential electron transport rate	J	μmol m^{-2} s^{-1}
Maximum potential electron transport rate (at 25 °C)	J_{max} (J_{max25})	μmol m^{-2} s^{-1}
Index for start of a subinterval of reference-comparison interval	k	–
Turnover number for RuBP carboxylation	k_c	s^{-1}
Michaelis constant for RuBP carboxylation (at 25 °C)	K_c (K_{c25})	μmol mol^{-1}
Turnover number for RuBP oxygenation	k_o	s^{-1}
Michaelis constant for RuBP oxygenation (at 25 °C)	K_o (K_{o25})	μmol mol^{-1}
Calculus-based relative limitations to A because of g_{sc}, g_m, V_{cmax}	l_s, l_{mc}, l_b	dimensionless
Averages of l_s, l_{mc} and l_b at reference and comparison points	$\overline{l}_s$, $\overline{l}_{mc}$, $\overline{l}_b$	dimensionless
Number of subintervals of reference-comparison interval	n	–
Number of variables that affect A	N	–
Ambient oxygen mole fraction	O	μmol mol^{-1}
Contribution of biochemical variables to a change in A	ρ_{bio}	%
Contribution of diffusional variables to a change in A	ρ_{diff}	%
Contribution of g_{m25} to a change in A	ρ_{gm25}	%
Contribution of g_{sc} to a change in A	ρ_{gsc}	%
Contribution of J_{max} (J_{max25}) to a change in A	ρ_{Jmax} (ρ_{Jmax25})	%
Contribution of K_c to a change in A	ρ_{Kc}	%
Contribution of R_d (R_{d25}) to a change in A	ρ_{Rd} (ρ_{Rd25})	%
Contribution of T to a change in A (for constant 25 °C values)	ρ_T	%
Contribution of T and 25 °C values together to a change in A	$\rho_{T,25}$	%
Contribution of V_{cmax} (V_{cmax25}) to a change in A	ρ_{Vcmax} ($\rho_{Vcmax25}$)	%
Contribution of an arbitrary variable x_j to a change in A	ρ_{xj}	%
Contribution of 25 °C values to a change in A (for constant T)	ρ_{25}	%
Convexity parameter for response of J to i (at 25 °C)	θ_j (θ_{j25})	dimensionless
Rate of non-photorespiratory CO_2 release (at 25 °C)	R_d (R_{d25})	μmol m^{-2} s^{-1}
Leaf temperature	T	°C
Maximum carboxylation rate (at 25 °C)	V_{cmax} (V_{cmax25})	μmol m^{-2} s^{-1}
Value of V_{cmax} at reference point (at comparison point)	$V_{cmax,R}$ ($V_{cmax,C}$)	μmol m^{-2} s^{-1}
Rate of triose phosphate utilization (at 25 °C)	V_{tpu} (V_{tpu25})	μmol m^{-2} s^{-1}
Arbitrary variable that affects A	x_j	varies
All variables that affect A except x_j, evaluated at index k	$\mathbf{x}_{-j,k}$	varies

$$\frac{A_{max,R}-A_{max,C}}{A_{max,R}} \approx \overline{l}_s\left(\frac{g_{sc,R}-g_{sc,C}}{g_{sc,R}}\right)+\overline{l}_{mc}\left(\frac{g_{m,R}-g_{m,C}}{g_{\mathbf{m},R}}\right) + \overline{l}_b\left(\frac{V_{cmax,R}-V_{cmax,C}}{V_{cmax,R}}\right), \quad (4)$$

where the subscripts R and C denote values at the reference and comparison points, respectively, and the overbars on l_s, l_{mc} and l_b indicate averages of values at these two points. The three groups of terms on the right-hand side of Eqn 4 are termed *contributions* (of g_{sc}, g_m and V_{cmax}, respectively) to the observed change in A_{max}.

Ideally, to apply Eqn 3 to finite changes, one would integrate this expression over the interval between the reference and comparison points. Equation 4 is a simple numerical approximation of that integral. However, Eqn 4 has some issues. One is that integrating Eqn 3 does not partition changes in A_{max} into contributions from changes in g_{sc}, g_m and

V_{cmax}; rather, it partitions changes in the natural logarithm of A_{max} into contributions from changes in the natural logarithms of g_{sc}, g_m and V_{cmax}. This is most easily seen by rewriting Eqn 3 as

$$d\ln A_{max} = l_s d\ln g_{sc} + l_{mc} d\ln g_m + l_b d\ln V_{cmax}. \quad (3a)$$

Alternatively, Eqn 4 could be interpreted as an estimate of the integral of Eqn 2 (which does partition changes in A_{max} itself), normalized by $A_{max,R}$. Even in that case, however, it is unclear whether the discrete approximation in Eqn 4 provides an unbiased estimate of that integral. Because of these issues, it is not clear whether Eqn 4 accurately partitions changes in A_{max} into contributions from the underlying variables.

The objectives of this paper were (1) to demonstrate that Eqn 4 does not accurately partition changes in A_{max}, by comparing its output with numerical integrals of Eqn 2; (2) to propose a revision of the GM approach, based on numerical integration, that resolves this issue; (3) to generalize the revised approach beyond light-saturated conditions, to encompass changes in any photosynthetic variable; (4) to demonstrate the generalized approach; and (5) to provide a user-friendly computational tool for applying the generalized approach.

METHODS

In this section, we first describe a series of simulated experiments designed to compare Eqn 4 with the numerical integral of Eqn 2 (normalized by $A_{max,R}$). We then describe our numerical integration approach. Finally, we describe a generalized partitioning approach based on numerical integration of Eqn 2.

Comparison of Eqn 4 with numerical integration of Eqn 2

We compared the partitioning calculated by Eqn 4 with that given by numerically integrating Eqn 2 and normalizing the result by $A_{max,R}$, in four series of simulated scenarios, each representing a change in A_{max} resulting from changes in g_{sc}, g_m and V_{cmax}. All scenarios shared the same reference state ($V_{cmax,R}$ = 150 μmol m^{-2} s^{-1} and $g_{sc,R} = g_{m,R}$ = 0.3 mol m^{-2} s^{-1}), but differed in the values of each variable in the comparison state; these scenarios are summarized in Table 2. In the first and second series of scenarios, V_{cmax} was reduced by two-thirds in the comparison state (relative to the reference state), and total conductance to CO_2 was reduced by amounts ranging from 0% (no change) to 83.3%. In the third and fourth series, total conductance was reduced by half while V_{cmax} was reduced by amounts ranging from 0 to 83.3%. The reductions in total conductance were achieved either by reducing g_{sc} and g_m by equal amounts in each scenario (in series 1 and 3) or by reducing only g_{sc} (in series 2 and 4). In each case, we computed A_{max} from the carboxylation-limited version of the Farquhar *et al.* (1980) photosynthesis model (for details, see Supporting Information Notes S1).

Table 2. Values of variables (carboxylation capacity, V_{cmax}; stomatal conductance to CO_2, g_{sc}; mesophyll conductance, g_m; total CO_2 conductance, g) used as the comparison state in the scenarios illustrated in Figs 2 and 3

Scenario series	Scenario	Value in comparison state			
		V_{cmax}	g_{sc}	g_m	g
1	1a	50	0.25	0.25	0.125
	1b	50	0.20	0.20	0.10
	1c	50	0.15	0.15	0.075
	1d	50	0.10	0.10	0.05
	1e	50	0.05	0.05	0.025
2	2a	50	0.214	0.3	0.125
	2b	50	0.15	0.3	0.10
	2c	50	0.10	0.3	0.075
	2d	50	0.06	0.3	0.05
	2e	50	0.027	0.3	0.025
3	3a	125	0.1	0.3	0.075
	3b	100	0.1	0.3	0.075
	3c	75	0.1	0.3	0.075
	3d	50	0.1	0.3	0.075
	3e	25	0.1	0.3	0.075
4	4a	125	0.15	0.15	0.075
	4b	100	0.15	0.15	0.075
	4c	75	0.15	0.15	0.075
	4d	50	0.15	0.15	0.075
	4e	25	0.15	0.15	0.075

Reference state values were $V_{cmax,R}$ = 150 μmol m^{-2} s^{-1} and $g_{sc,R} = g_{m,R}$ = 0.30 mol m^{-2} s^{-1} (g = 0.15 mol m^{-2} s^{-1}).

Numerical integration of Eqn 2

For the scenarios described earlier, we estimated the integral of Eqn 2 numerically:

$$\int_R^C dA_{max} = \int_R^C \left(\frac{\partial A_{max}}{\partial g_{sc}}\right) dg_{sc} + \int_R^C \left(\frac{\partial A_{max}}{\partial g_m}\right) dg_m + \int_R^C \left(\frac{\partial A_{max}}{\partial V_{cmax}}\right) dV_{cmax}, \quad (5)$$

where the limits of integration ('*R*' and '*C*') refer to the reference and comparison points, respectively. The three integrals on the right-hand side of Eqn 5 represent the contributions of g_{sc}, g_m and V_{cmax}, respectively, to the change in A between the reference and comparison points. These integrals can be estimated numerically by approximating the differentials and derivatives therein as finite differences and ratios of finite differences, respectively. For example, for the term in Eqn 2 involving g_{sc}:

$$\int_R^C \left(\frac{\partial A_{max}}{\partial g_{sc}}\right) dg_{sc} \approx \sum_{k=0}^{n-1} \left(\left.\frac{\Delta A_{max}}{\Delta g_{sc}}\right|_{g_m, V_{cmax}}^{k,k+1}\right) \cdot \Delta g_{sc} = \sum_{k=0}^{n-1} \left(\Delta A_{max}|_{g_m, V_{cmax}}^{k,k+1}\right), \quad (5a)$$

where the summation occurs over n equal subdivisions of the interval between the reference and comparison points (k = 0 and n, respectively); the superscript 'k, k+1' means that the changes ΔA_{max} and Δg_{sc} are computed between indices k and k+1; and the subscript 'g_m,V_{cmax}' indicates that ΔA_{max} is computed by changing g_{sc} while holding g_m and V_{cmax} constant.

This change in A_{max} could be estimated by computing $\partial A_{max}/\partial g_{sc}$ analytically and multiplying it by a small finite increment in g_{sc}, but it can be computed more easily and directly by simply changing g_{sc} in the photosynthesis model. For example, Eqn 5 becomes

$$= \sum_{k=0}^{n-1} [A_{max}(g_{sc,k+1}, g_{m,k}, V_{cmax,k}) - A_{max}(g_{sc,k}, g_{m,k}, V_{cmax,k})], \quad (5b)$$

where $A_{max}(g_{sc,k}, g_{m,k}, V_{cmax,k})$ refers to the carboxylation-limited form of the photosynthesis model, evaluated at the values of g_{sc}, g_m and V_{cmax} indicated by the index k. An example of the application of Eqn 5 is described in Table 3 and illustrated in Fig. 1. This approach avoids partial derivatives altogether, which greatly simplifies its generalization to other variables (as shown later).

For clarity, we adopt the following simplified and generalized notation:

$$[\delta A|\delta x_j]_k^{k+1} \equiv A(x_{j,k+1}, \mathbf{x}_{-j,k}) - A(x_{j,k}, \mathbf{x}_{-j,k}), \quad (6)$$

where $\mathbf{x}_{-j}$ means 'all variables other than x_j' ('¬' means 'not'). In the notation on the left hand side of Eqn 6, variables that appear after the vertical bar are allowed to change, and all other variables are held constant. Equation 5 thus becomes

$$\int_R^C \left(\frac{\partial A_{max}}{\partial g_{sc}}\right) dg_{sc} \approx \sum_{k=0}^{n-1} [\delta A_{max}|\delta g_{sc}]_k^{k+1}. \quad (5c)$$

The other terms in Eqn 2 (those involving g_m and V_{cmax}) are integrated in the same manner as shown in Eqn 5c.

The numerical integration represented by Eqn 5 requires an assumption about how g_{sc}, g_m and V_{cmax} vary across the interval – that is, about the 'paths' taken by these variables between the reference and comparison points. The simplest assumption, which we adopt here, is that the variables change at a uniform rate (i.e., linearly with 'time', if the interval is understood to represent a period of time). Thus, $g_{sc,k} = g_{sc,R} + k \cdot (g_{sc,C} - g_{sc,R})/n$, and likewise for $g_{m,k}$ and $V_{cmax,k}$. We note that GM also assumes paths for each variable: Eqn 4 represents an approximate integral of Eqn 2 (cf. their Eqns 6 and 8), and Eqn 2 cannot be integrated without specifying such paths. The key difference is that our approach clearly and explicitly identifies these paths.

Note that Eqn 5 gives contributions with the opposite sign to those calculated by Eqn 4 (because Eqn 5 treats the reference point as the lower integration bound), so when comparing these equations, we multiplied the output of Eqn 5 by minus 1. However, the generalized approach described later retains the sign convention of Eqn 5.

Generalization of the revised approach

We propose a generalized approach to partitioning changes in A into contributions from the underlying variables. In this new approach, Eqn 2 is numerically integrated across the interval between reference and comparison points and the resulting contributions are expressed as percentages of the reference value of A (A_{ref}). The contribution from a variable x_j to a change in A is defined as

$$\rho_{xj} \equiv \frac{100}{A_{ref}} \cdot \sum_{k=0}^{n-1} [\delta A|\delta x_j]_k^{k+1}. \quad (7)$$

Because this approach does not use partial derivatives, but instead computes partial changes in A directly from the photosynthesis model, it is easily generalized to arbitrary conditions (such as sub-saturating photosynthetic photon flux, PPF) and to variables other than g_{sc}, g_m and V_{cmax}. The generalization is most clearly presented by expressing A as a function of many variables:

Table 3. Example application (also illustrated in Fig. 1) of the method presented in this paper for partitioning changes in A (μmol m^{-2} s^{-1}) into contributions from the underlying variables

		Values					
Description	Symbol or expression	(Ref)				(Comp)	Total change
Index of sub-interval	k	0	1	2	3	4	
g_{sc} at start of sub-interval	$g_{sc,k}$	0.3	0.23	0.16	0.1	0.03	
V_{cmax} at start of sub-interval	$V_{cmax,k}$	150	125	100	75	50	
A at start of sub-interval	$A(g_{sc,k}, V_{cmax,k})$	26.5	22.5	18.0	12.7	5.5	
A at new g_{sc}	$A(g_{sc,k+1}, V_{cmax,k})$	24.6	20.1	14.6	6.2		
A at new V_{cmax}	$A(g_{sc,k}, V_{cmax,k+1})$	24.0	19.8	15.1	10.0		
Change in A because of g_{sc}	$A(g_{sc,k+1}, V_{cmax,k}) - A(g_{sc,k}, V_{cmax,k})$	–1.9	–2.4	–3.4	–6.5		–14.1
Change in A because of V_{cmax}	$A(g_{sc,k}, V_{cmax,k+1}) - A(g_{sc,k}, V_{cmax,k})$	–2.5	–2.7	–2.8	–2.8		–10.8
Actual change in A	$A(g_{sc,k+1}, V_{cmax,k+1}) - A(g_{sc,k}, V_{cmax,k})$	–4	–4.5	–5.2	–7.2		–21
% contribution from g_{sc}	100 · (change due to g_{sc})/(reference value of A)						–53.1%
% contribution from V_{cmax}	100 · (change due to V_{cmax})/(reference value of A)						–40.7%

In this example, it is assumed that only two variables (g_{sc} and V_{cmax}) change between the reference ('ref') and comparison ('comp') points, from 0.3 to 0.027 mol m^{-2} s^{-1} (g_{sc}) and from 150 to 50 μmol m^{-2} s^{-1} (V_{cmax}). The interval between those points is divided into n sub-intervals ($n = 4$ in this example), whose starting and ending points are indicated by the index k. Partial changes in A between each successive sub-interval are calculated based on the corresponding changes in g_{sc} and V_{cmax}, and the contributions are calculated based on the sums of these changes, as shown. We recommend using $n = 1000$.

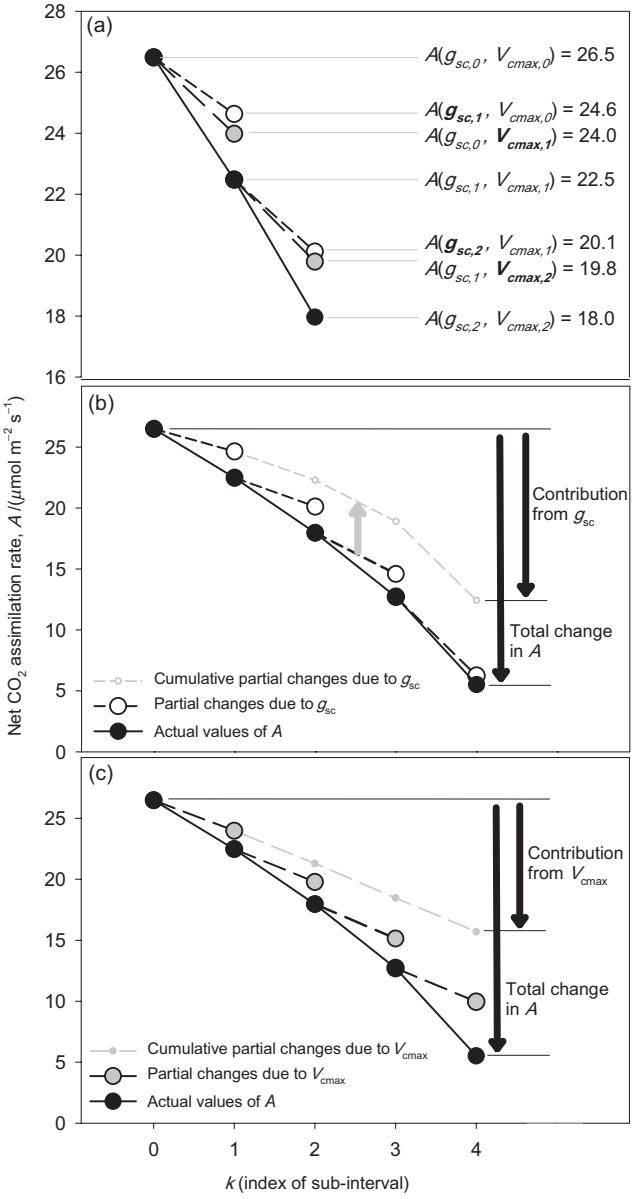

Figure 1. Example illustrating the sequence of partial and total changes in A because of changes in g_{sc} and V_{cmax}, calculated for sub-intervals of a total interval between reference and comparison conditions. In this example, the reference-to-comparison interval is divided into four sub-intervals, denoted by the index k; the reference and comparison points correspond to $k = 0$ and $k = 4$, respectively. The values shown in this figure correspond to the example detailed in Table 3. (a) Example showing values of A calculated at the first three points in the interval ($k = 0$, 1 and 2), and the corresponding values of A calculated by changing only g_{sc} (white symbols, short-dashed lines), or by changing only V_{cmax} (grey symbols, long-dashed lines) across each successive sub-interval. Note that the initial condition for each of these 'partial changes' in A is the actual value of A at the start of the sub-interval. (b) Values of A (solid symbols, solid line), partial changes in A because of g_{sc} (large white symbols, short-dashed black line), and an imaginary sequence of A that would result from accumulating only the partial changes in A because of g_{sc} (small white symbols, grey dashed line). (c) Values of A (solid symbols, solid line), partial changes in A because of V_{cmax} (large grey symbols, long-dashed black line), and an imaginary sequence of A that would result from accumulating only the partial changes in A because of V_{cmax} (small grey symbols, grey dashed line). In (a), values of A at each point are given for cross-referencing with Table 3. In (b), an upward grey arrow is shown for one of the partial changes, to illustrate that the segments in the grey dashed line correspond to the partial changes. In (b) and (c), the sum of partial changes in g_{sc} and V_{cmax}, respectively, are shown by the shorter black arrows ('contributions'), and the total changes in A are shown by the longer black arrows.

$$A = A\left(\begin{matrix} g_{sc}, g_{bc}, g_m, V_{cmax}, J_{max}, V_{tpu}, \\ R_d, K_c, \Gamma_*, \phi, \theta_j, c_a, O, i \end{matrix}\right), \tag{8}$$

where g_{bc} is boundary layer conductance to CO_2; J_{max} is maximum potential electron transport rate; V_{tpu} is triose phosphate utilization (TPU) rate; R_d is the rate of non-photorespiratory CO_2 release; K_c and K_o are the Michaelis constants for ribulose-1,5-bisphosphate (RuBP) carboxylation and oxygenation, respectively; Γ_* is the photorespiratory CO_2 compensation point; i is PPF; ϕ is the initial slope of the response of potential electron transport rate (J) to i; θ_j is a dimensionless convexity parameter for the response of J to i; c_a is ambient CO_2 concentration; and O is ambient O_2 concentration. (Note that Γ_* is not independent of K_c, K_o and O in the original Farquhar *et al.* (1980) model, but is given by $\Gamma_* = O\,K_c\,k_o/(2K_o\,k_c)$, where k_o and k_c are the Rubisco turnover numbers for RuBP oxygenation and carboxylation, respectively. In practice, investigators often treat Γ_* as an empirical parameter. Users preferring the initial formulation should replace Γ_* with k_c and k_o in Eqn 8. Note also that Eqn 8 omits the influence of the evaporative gradient, which, together with g_{sc} and g_{bc}, determines transpiration rate; the latter in turn affects A via ternary interactions between H_2O and CO_2.)

An alternative formulation that separates the effects of temperature (T) and 25 °C values of T-dependent variables is shown in Eqn 9.

$$A_{25T} = A_{25T}\left(\begin{matrix} g_{sc}, g_{bc}, g_{m25}, V_{cmax25}, J_{max25}, V_{tpu25}, R_{d25}, \\ K_{c25}, K_{o25}, \Gamma_{*25}, \phi_{25}, \theta_{j25}, c_{a25}, pO_2, i, T \end{matrix}\right). \tag{9}$$

The contribution from a change in the 25 °C value (x_{j25}) of a variable x_j, independent of changes in T, can then be defined as

$$\rho_{xj25} \equiv \frac{100}{A_{ref}} \cdot \sum_{k=0}^{n-1} [\delta A_{25T} | \delta x_{j25}]_k^{k+1}, \tag{10}$$

and the total contribution from changes in all 25 °C values *per se* is

$$\rho_{25} \equiv \frac{100}{A_{ref}} \cdot \sum_{k=0}^{n-1} \left[\begin{matrix} \delta A_{25T} | \delta g_{m25}, \delta V_{cmax25}, \delta J_{max25}, \delta V_{tpu25}, \delta R_{d25}, \\ \delta K_{c25}, \delta K_{o25}, \delta \Gamma_{*25}, \delta \phi_{25}, \delta \theta_{j25} \end{matrix}\right]. \tag{11}$$

The contribution from *T per se* (ρ_T), independent of changes in 25 °C values, is

$$\rho_T \equiv \frac{100}{A_{ref}} \cdot \sum_{k=0}^{n-1} [\delta A_{25T} | \delta T]_k^{k+1}. \quad (12)$$

A distinct notation (A_{25T}) is used to represent the functional form of A given in Eqn 9 and relevant to Eqns 12 and 11, to clarify that it is the 25 °C values of T-dependent variables, and not their temperature-adjusted values, that are held constant when computing ρ_T. An *overall* contribution from temperature, including both the direct effect of T and changes in 25 °C values, can be defined as

$$\rho_{T,25} \equiv \frac{100}{A_{ref}} \cdot \sum_{k=0}^{n-1} \left[\delta A | \delta g_m, \delta V_{c\,max}, \delta J_{max}, \delta V_{tpu}, \delta R_d, \delta K_c, \delta K_o, \delta \Gamma_*, \delta \phi, \delta \theta_j \right]_k^{k+1}. \quad (13)$$

Similarly, the total contribution from diffusional conductances (g_{sc}, g_m and g_{bc}) is

$$\rho_{diff} \equiv \frac{100}{A_{ref}} \cdot \sum_{k=0}^{n-1} [\delta A | \delta g_{sc}, \delta g_{bc}, \delta g_m]_k^{k+1}, \quad (14)$$

and the total contribution from variables that involve the biochemistry of photosynthesis is

$$\rho_{bio} \equiv \frac{100}{A_{ref}} \cdot \sum_{k=0}^{n-1} \left[\delta A | \delta V_{c\,max}, \delta J_{max}, \delta V_{tpu}, \delta R_d, \delta K_c, \delta K_o, \delta \Gamma_*, \delta \phi, \delta \theta_j, \delta i \right]_k^{k+1}. \quad (15)$$

We include the effect of PPF (i) in ρ_{bio} because the direct effect of i on A occurs via J, which is usually viewed as a biochemical variable.

Demonstration of the generalized approach

We applied Eqns 7 and 12–15 to field measurements of leaf gas exchange in olive (*Olea europaea* L.) trees, performed in 2002 and partially published in 2007 (Diaz-Espejo *et al.* 2007). We measured responses of A to intercellular CO_2 mole fraction (c_i) and diurnal cycles of leaf gas exchange at two canopy positions (east- and west-facing) in four trees under two watering treatments (well-watered and water-stressed), in two seasons (April and August) (for details, see Diaz-Espejo *et al.* 2007). Both positions had similar daily-integrated PPF, but different patterns of air humidity, temperature and time of peak PPF.

All measurements used a portable photosynthesis system (LI-6400, Li-Cor, Lincoln, NE, USA) with a 2×3 cm broadleaf chamber and an integrated light source (LI-6400-02B; Li-Cor). We estimated V_{cmax}, J_{max}, TPU and g_m by fitting the photosynthesis model of Farquhar *et al.* (1980) to A versus c_i curves, following the curve-fitting method proposed by Ethier & Livingston (2004). The curves were performed under saturating PPF (1600 μmol m^{-2} s^{-1}) and constant leaf temperature (20 °C in April and 25 °C in August) by changing the CO_2 concentration of inlet air in 11 steps from 50 to 1400 μmol mol^{-1} (see Díaz-Espejo *et al.* 2006 for details). Curves were measured for six leaves per treatment, per canopy position in April 2002, and four leaves per treatment and position in August 2002. Diurnal cycles of A and g_s *in situ* (seven measurements per day) were measured in August on 12 leaves (three per tree × four trees) per treatment and canopy position, and the results were averaged within each treatment/position pair. Temperature dependencies of photosynthetic parameters were calculated according to Bernacchi *et al.* (2002), using parameters specifically determined for olive leaves (Díaz-Espejo *et al.* 2006) and modified to account for the effect of g_m (for details, see Supporting Information Notes S1).

We defined the reference point as the point at which A was greatest; this was always April for seasonal changes, but it varied among treatments for diurnal cycles.

Numerical procedures

We implemented the calculations described earlier using worksheet and user-defined functions and Visual Basic for Applications (VBA) subroutines in a Microsoft Excel 2010 spreadsheet (Microsoft Corp., Redmond, WA, USA), which is included as Supporting Information Notes S2, and is available from the authors upon request.

RESULTS

Choice of number of steps for numerical integration

To quantify the trade-off between speed and accuracy in numerical integration of Eqn 2, we computed the sum of contributions to seasonal changes in A for all variables in the four field treatments described earlier, for a range of values of n (the number of numerical integration steps). We estimated the true value of each integral as its numerical integral using $n = 30{,}000$. The percentage error of numerical integration declined as the inverse of n ($\ln|\%\ \text{error}| = -0.98 \ln|n| + 3.32$; adjusted $r^2 = 0.96$, $P < 0.0001$, degrees of freedom = 74; not shown). For $n = 1000$, the error was less than 0.07% across datasets, and the calculations took 1.3 s per comparison point on a modern personal computer with many other programs running. We conclude that numerical integration with $n = 1000$ is adequate and feasible, and we used $n = 1000$ for all calculations presented here.

Comparison of Eqn 4 (the GM approach) with numerical integration of Eqn 2

Equation 4 systematically underestimated the percentage contributions of V_{cmax} and g_{sc} to simulated changes in A_{max} (Figs 2 & 3). The degree of underestimation differed if a given decrease in total CO_2 conductance was effected by reducing both g_{sc} and g_m (scenario series 1 and 3) or by reducing only g_{sc} (scenario series 2 and 4) (e.g. compare Fig. 2a,c and Fig. 2b,d, or Fig. 3a,c and Fig. 3b,d). Furthermore, the contributions calculated using Eqn 4 were non-linearly related to those computed by numerical integration. For example, Eqn 4 underestimated the g_{sc} contribution by

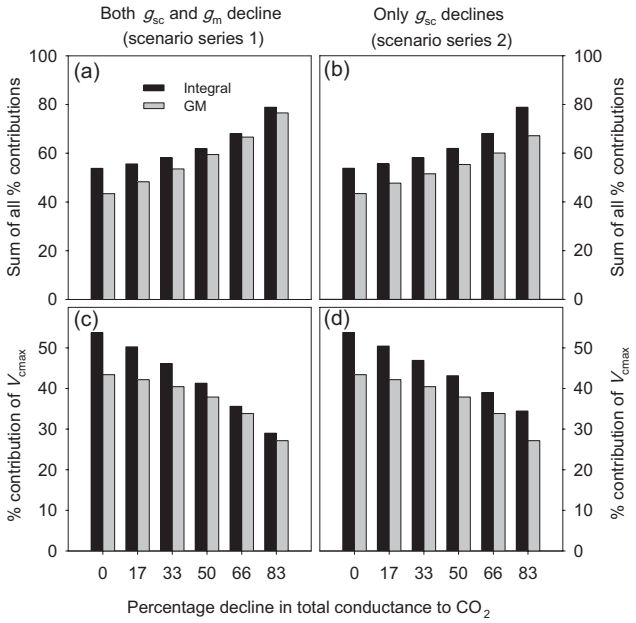

Figure 2. Comparison of contributions to changes in A_{max} computed using the GM approach (Eqn 4) (grey bars, 'GM') or by numerically integrating Eqn 2 (black bars, 'integral'), for different scenarios in which total CO_2 conductance was reduced by different percentages (horizontal axis), either by reducing both stomatal conductance (g_{sc}) and mesophyll conductance (g_m) equally (panels a and c; scenario series 1) or by reducing only g_{sc} (panels b and d; scenario series 2). (a,b) The sum of contributions from all variables combined. (c,d) The contribution from V_{cmax}. Scenarios are described in the text and summarized in Table 2.

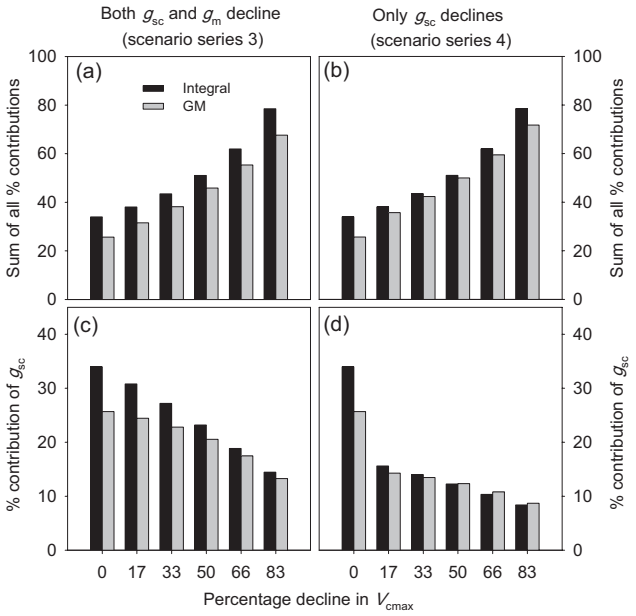

Figure 3. Comparison of contributions to changes in A_{max} computed using the GM approach (Eqn 4) (grey bars, 'GM') or by numerically integrating Eqn 2 (black bars, 'integral'), for different scenarios in which carboxylation capacity (V_{cmax}) was reduced by different percentages (horizontal axis), and total CO_2 conductance was reduced by half, either by reducing both stomatal conductance (g_{sc}) and mesophyll conductance (g_m) equally (panels a and c; scenario series 3) or by reducing only g_{sc} (panels b and d; scenario series 4). (a,b) The sum of contributions from all variables combined. (c,d) The contribution from g_{sc}. Scenarios are described in the text and summarized in Table 2.

24.5% when V_{cmax} was identical in the reference and comparison states, but by 8.1% when V_{cmax} decreased by 83% in the comparison state (Fig. 3c). These results demonstrate that Eqn 4 is a biased tool for partitioning changes in A_{max}.

Demonstration of the generalized approach for seasonal changes

Figure 4a shows the contributions estimated using the new approach. The corresponding 25 °C values of V_{cmax}, J_{max}, R_d and g_m, and the observed values of g_{sc}, are given in Table 4.

Total relative changes in A were greater under water stress, mainly because of greater stomatal contributions: ρ_{gsc} was positive in well-watered conditions (+6.7 to +11.8%) because g_{sc} increased from April to August (Table 4), whereas ρ_{gsc} was negative under water stress (−14.6 to −23.9%; red bars in Fig. 4a). The contribution from g_m (including the effects of changes in its 25 °C value and changes in temperature) was negative in all treatments, but was generally smaller than the stomatal contribution, ranging from −3.0 to −9.0%. ρ_{Vcmax} was similar in magnitude to ρ_{gsc}, but was always negative (−11.3 to −24.7%).

Table 4. Values of photosynthetic variables in April (reference point, 'ref') and August (comparison point, 'comp') in the four experimental treatments (well-watered versus water-stressed, and east- versus west-facing sections of an olive canopy) used to demonstrate the generalized approach for seasonal changes

	Well-watered				Water-stressed			
	East-facing		West-facing		East-facing		West-facing	
Variable	Ref	Comp	Ref	Comp	Ref	Comp	Ref	Comp
V_{cmax25}	160.3	74.0	168.3	75.8	169.0	83.2	168.6	49.9
J_{max25}	186.8	212.2	223.6	213.4	292.3	214.5	290.2	215.6
R_{d25}	1.2	3.0	1.6	4.0	2.1	6.0	2.8	5.0
g_{m25}	0.331	0.163	0.337	0.204	0.335	0.149	0.371	0.117
g_{sc}	0.135	0.156	0.117	0.166	0.154	0.093	0.179	0.058

For photosynthetic variables not listed here, values were not independently measured across treatments, and assumed values are given in the Supporting Information Notes S1. Units for V_{cmax25}, J_{max25} and R_{d25} are μmol m^{-2} s^{-1}, and units for g_{m25} and g_{sc} are mol m^{-2} s^{-1}.

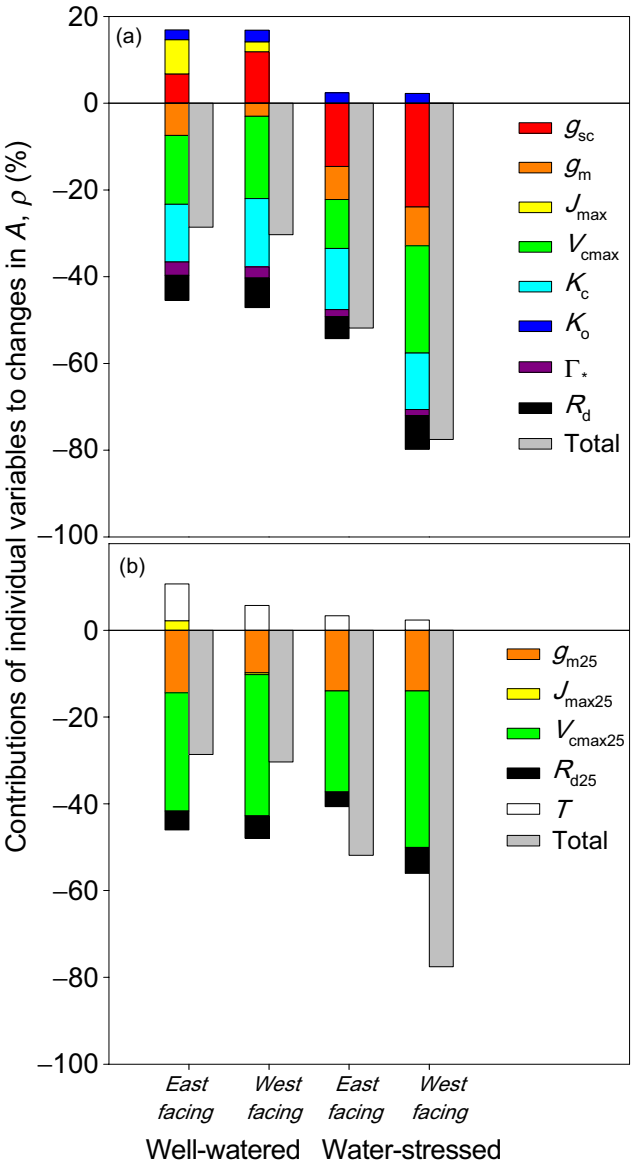

Figure 4. Contributions of individual variables (ρ) to seasonal changes in light-saturated net CO_2 assimilation rate (A_{max}) across four treatments as shown below the horizontal axis, with the reference point taken as spring measurements (April) and the comparison point taken as late summer measurements (August). (a) Contributions from total changes in each variable, including effects of temperature and changes in values of variables at 25 °C (for g_m, J_{max}, V_{cmax} and R_d). (b) Contributions from changes in values at 25 °C (g_{m25}, J_{max25}, V_{cmax25} and R_{d25}), and the total contribution from changes in temperature (T) calculated while holding 25 °C values constant. 'Total' refers to the total relative change in A, which equals the sum of contributions for all variables).

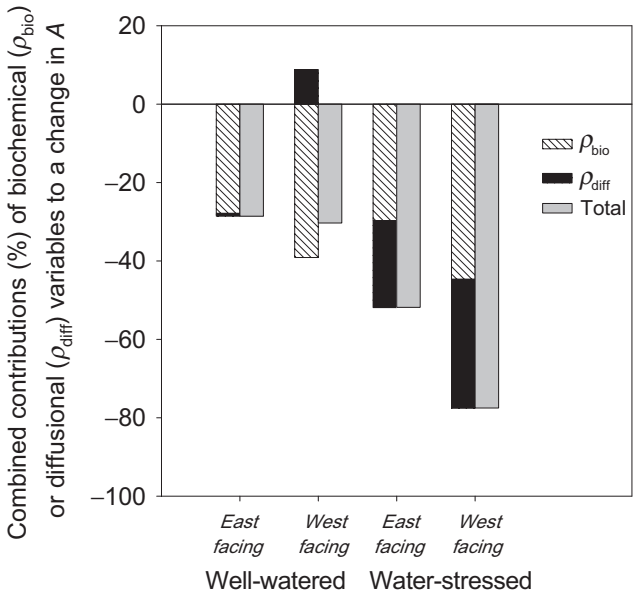

Figure 5. Contributions of groups of variables (ρ) to seasonal changes in light-saturated net CO_2 assimilation rate (A_{max}) across four treatments, with the reference point taken as spring measurements (April) and the comparison point taken as late summer measurements (August). 'bio', white bars with hatching: total contribution from changes in variables of photosynthetic biochemistry (J_{max}, V_{cmax}, K_c, K_o, Γ_*, R_d and i). 'diff', black bars: total contribution from changes in diffusional variables (g_{sc} and g_m). Other variables included in ρ_{bio} and ρ_{diff} in their respective definitions in the text were assumed or observed to be constant among treatments. 'Total', grey bars: the total relative change in A_{max}, which equals the sum of contributions for all variables.

Substantial fractions of the total seasonal changes in A were due to changes in variables other than g_{sc}, g_m and V_{cmax}. For example, the contributions from K_c and R_d ranged from −13.0 to −15.8% (for K_c) and from −5.1 to −7.8% (for R_d). The contribution from J_{max} was positive in the well-watered treatment (+2.3 to +7.9%), but 0 under water stress (because photosynthesis was carboxylation-limited in both seasons).

Figure 4b shows the contributions from temperature-related variables separated into the effects of changes in T *per se* (calculated while holding 25 °C values constant) and changes in 25 °C values. The direct effect of T was small, but positive in each case, ranging from +2.4 to +8.5% (because measurement T was slightly higher in August), whereas the total contribution from 25 °C values was large and negative, ranging from −40.6 to −56.0%. This was largely driven by large seasonal decreases in the value of V_{cmax} at 25 °C, but also by increases in the value of R_d at 25 °C.

Figure 5 shows the combined contributions from seasonal changes in all diffusional variables (ρ_{diff}) and all biochemical variables (ρ_{bio}). ρ_{diff} was negligible in the east-facing well-watered treatment, positive in the west-facing well-watered treatment, and large and negative in both water-stressed treatments. By contrast, ρ_{bio} was large and negative, and greater in magnitude than p_{diff}, in all cases.

Demonstration of the generalized approach for diurnal changes

The diurnal trends in A, g_{sc}, g_m, T and i observed in August are shown in Fig. 6, and the associated contributions are shown in

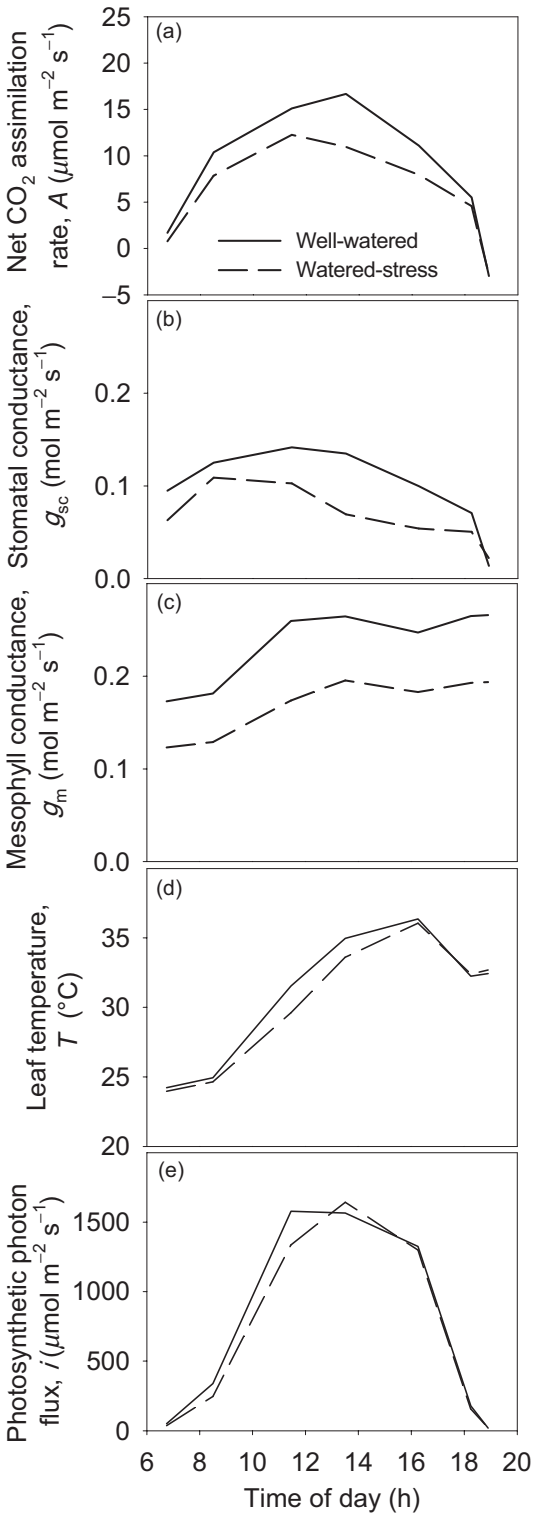

Figure 6. Diurnal changes in (a) net assimilation rate; (b) stomatal conductance; (c) mesophyll conductance; (d) temperature; and (e) photosynthetic photon flux, in well-watered (solid lines) and water-stressed (dashed lines) treatments in olive.

Figs 7 and 8 for well-watered and water-stressed conditions, respectively. In each figure, ρ_{diff} and ρ_{bio} are presented in panel (a) and broken down into individual variables in panels (b) – (e). Low PPF caused ρ_{bio} to dominate in the morning, whereas ρ_{bio} and ρ_{diff} were similar late in the day (Figs 7a & 8a). Late-day diffusional suppression of A was entirely due to g_{sc} (Figs 7b & 8b). The effect of biochemical variables other than PPF was small across the day (Figs 7c & 8c). This reflected a fine balance among the effects of several variables, particularly between V_{cmax} and K_c: ρ_{Vcmax} was negative in the morning and positive in the afternoon (Figs 7d & 8d), but this was opposed by a similar, but reverse trend in ρ_{Kc} (Figs 7e & 8e).

DISCUSSION

Comparison of our approach with that of Grassi & Magnani (2005)

The approach presented earlier for partitioning changes in A into components because of the underlying variables uses numerical integration (e.g. Eqn 5) rather than discrete approximations of differentials and partial derivatives (cf. Eqn 4). Our approach has two major advantages: it avoids the bias caused by the discrete approximations in Eqn 4 (Figs 2 & 3), and by avoiding the need to compute partial derivatives for each variable and relying instead on substitution in the photosynthesis model, our approach is easily extended to encompass effects of changes in any photosynthetic variable, under any conditions. This extension also allows the total contribution of changes in temperature to be calculated, including both the direct effect of T and the effect of changes in 25 °C values. This total effect may be more relevant for quantifying the adaptive significance of seasonal changes in photosynthetic parameters such as V_{cmax}, because selection acts more directly on temperature-adjusted parameters than on their 25 °C values.

A constraint of the new approach is that it requires a fully parameterized photosynthesis model. However, only three additional parameters (J_{max}, R_d and g_{bc}) are required beyond those needed to apply the method of Grassi & Magnani (2005), and these three parameters are typically measured or estimated in the same procedures used to estimate V_{cmax}. Both methods rely on calculations based on a model (to compute its derivatives in the GM approach or to compute small changes by direct substitution in our approach), so both methods are only meaningful to the extent that the model adequately describes how each variable affects A.

The terminology associated with photosynthetic limitations analysis is sometimes ambiguous. For example, 'limitations' is used to describe both the contributions of changes in variables to a change in A, and the extent to which A is limited by those variables at a given condition, irrespective of comparisons with any other measured condition (e.g. Farquhar & Sharkey 1982). To avoid ambiguity, we recommend using the term 'contributions' to describe the quantities calculated by our method.

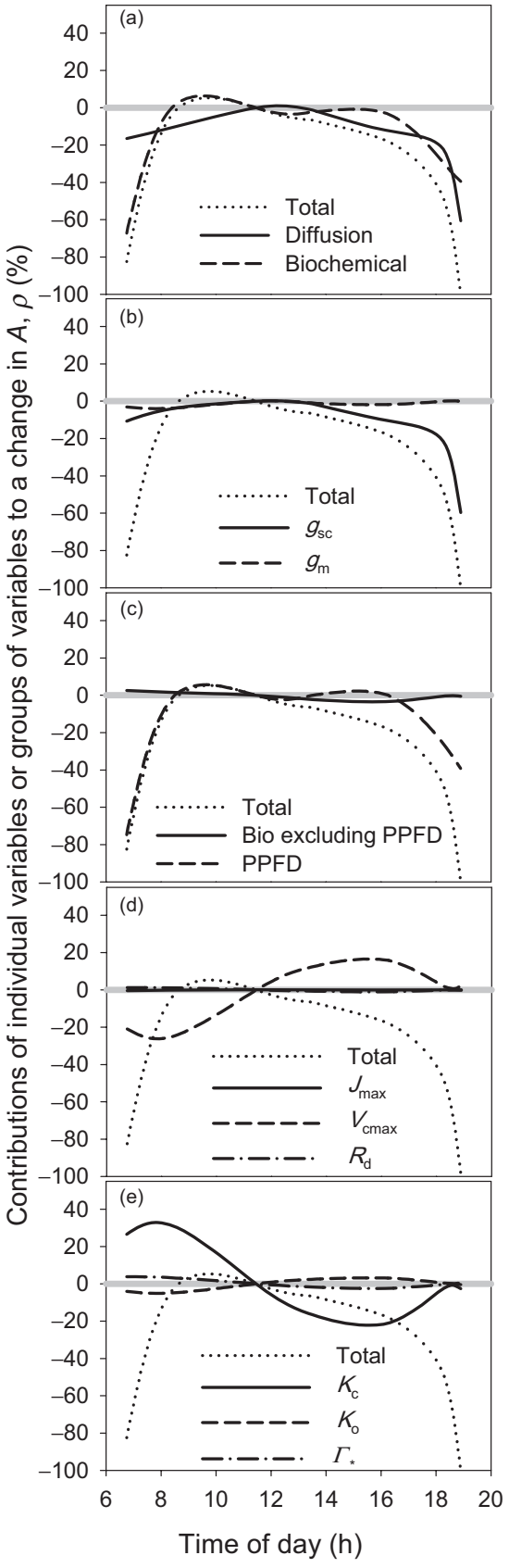

Figure 7. Contributions of individual variables and groups of variables to diurnal changes in net CO_2 assimilation rate (A) under well-watered conditions in olive, with the reference point taken as the time of day at which A was greatest. In each panel, the total relative change in A, which equals the sum of contributions for all variables, is shown with dotted lines ('Total') for reference. Grey horizontal lines represent zero on the vertical axis. (a) Total contribution from diffusional variables (ρ_{diff}, solid line) and biochemical variables (ρ_{bio}, dashed line). (b) Components of ρ_{diff}: ρ_{gsc} (solid line) and ρ_{gm} (dashed line). (c–e) Components of ρ_{bio}: (c) All components of ρ_{bio} except the component because of photosynthetic photon flux (PPF), ρ_i ('bio excluding PPF', solid line), and ρ_i ('PPF', dashed line). (d) Components of ρ_{bio} with flux dimensions: ρ_{Jmax} (solid line), ρ_{Vcmax} (dashed line) and ρ_{Rd} (dash-dot line). (e) Kinetic components of ρ_{bio}: ρ_{Kc} (solid line), ρ_{Ko} (dashed line) and $\rho_{\Gamma*}$ (dash-dot line).

Issue of path dependence

Jones (1985) noted that explicit integration of Eqn 2, which is the basis of our method, 'generally will not be feasible, because of a lack of detailed information both on the function $A(\ldots)$ and on the actual path followed between [the reference and comparison conditions].' The first challenge has since been overcome by the universal adoption of the Farquhar *et al.* (1980) photosynthesis model, combined with the ubiquity of gas exchange systems that allow its parameters to be estimated. We argue that the second challenge is not especially relevant to the questions that most investigators ask when they seek to partition changes in A. Although a path of change in each variable is indeed required to compute the integral, it is doubtful that most users are interested in how the variable's *actual* path would affect its calculated contribution to a change in A. Our method adopts the simplest assumption, which is that each variable changes at a uniform rate between the reference and comparison points. This allows contributions to be calculated in a standardized and unambiguous way.

One issue that can arise with this approach is that the results depend on whether the effect of stomata is expressed as a conductance (g_{sc}) or a resistance ($r_{sc} = g_{sc}^{-1}$), because linear changes in g_{sc} and r_{sc} give different sequences of physiological states. For example, suppose g_{sc} changes from 0.5 to 0.1 mol m^{-2} s^{-1}. The value of g_{sc} at the midpoint of the interval is 0.3 if g_{sc} changes linearly, but 0.17 if r_{sc} changes linearly (from 2 to 10 m^2 s mol^{-1}). However, most modern work in this field uses stomatal conductance rather than resistance, perhaps because both g_{sc} and V_{cmax} are positively related to limiting photosynthetic resources (the rate of water loss, and the photosynthetic nitrogen allocated to Rubisco, respectively), so the issue probably has little impact. At any rate, a similar issue would also arise if r_{sc} were used in place of g_{sc} in the GM method – indeed, changes in A cannot be unambiguously partitioned into changes due to the underlying variables without specifying paths for those variables, because Eqns 1 and 2 cannot be integrated without specifying paths. A strength of our approach is that it clearly and explicitly specifies these paths.

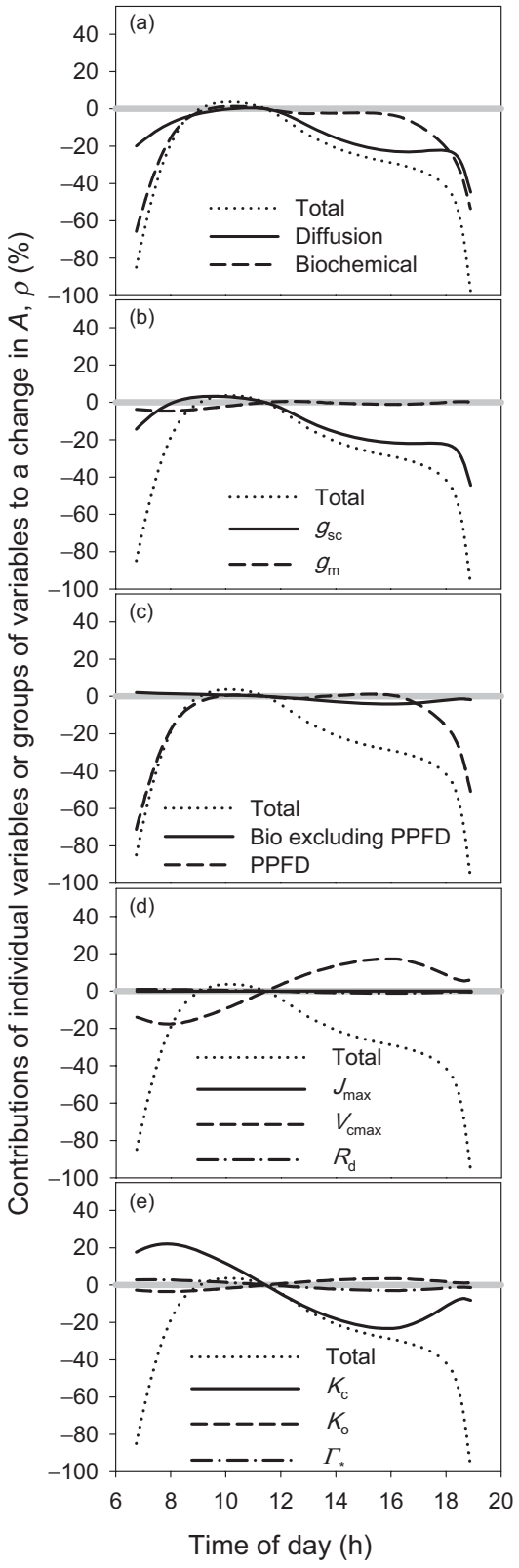

Figure 8. Contributions to diurnal changes in net CO_2 assimilation rate (A) in olive (as in Fig. 7, but for measurements made under water-stressed conditions).

Conclusion

The ubiquity of powerful desktop computing and an easily parameterized biophysical photosynthesis model obviate the approximations that were necessary in the past to partition changes in A. The direct, computationally intensive approach proposed here is now practical. We suggest further that our method is preferable to alternative methods that attempt to partition changes in A by coarsely approximating the integral of its exact differential (Eqn 1) using partial derivatives which yields biased and ambiguous partitioning.

ACKNOWLEDGMENTS

T.N.B. was funded by the Grains Research and Development Corporation (GRDC), the Australian Research Council (Award LP130101183) and the US National Science Foundation (Award #1146514). This work was funded by the Spanish Ministry of Science and Innovation (research project AGL2012-34544).

REFERENCES

Bernacchi C.J., Portis A.R., Nakano H., von Caemmerer S. & Long S.P. (2002) Temperature response of mesophyll conductance. Implications for the determination of Rubisco enzyme kinetics and for limitations to photosynthesis in vivo. *Plant Physiology* **130,** 1992–1998.

Díaz-Espejo A., Walcroft A., Fernández J., Hafidi B., Palomo M. & Girón I. (2006) Modeling photosynthesis in olive leaves under drought conditions. *Tree Physiology* **26,** 1445–1456.

Diaz-Espejo A., Nicolas E. & Fernandez J.E. (2007) Seasonal evolution of diffusional limitations and photosynthetic capacity in olive under drought. *Plant, Cell & Environment* **30,** 922–933.

Egea G., Verhoef A. & Vidale P.L. (2011) Towards an improved and more flexible representation of water stress in coupled photosynthesis–stomatal conductance models. *Agricultural and Forest Meteorology* **151,** 1370–1384.

Ethier G. & Livingston N. (2004) On the need to incorporate sensitivity to CO2 transfer conductance into the Farquhar–von Caemmerer–Berry leaf photosynthesis model. *Plant, Cell & Environment* **27,** 137–153.

Farquhar G.D. & Sharkey T.D. (1982) Stomatal conductance and photosynthesis. *Annual Review of Plant Physiology* **33,** 317–345.

Farquhar G.D., von Caemmerer S. & Berry J.A. (1980) A biochemical model of photosynthetic CO_2 assimilation in leaves of C_3 species. *Planta* **149,** 78–90.

Flexas J., Bota J., Galmes J., Medrano H. & Ribas-Carbó M. (2006a) Keeping a positive carbon balance under adverse conditions: responses of photosynthesis and respiration to water stress. *Physiologia Plantarum* **127,** 343–352.

Flexas J., Ribas-Carbó M., Bota J., Galmés J., Henkle M., Martínez-Cañellas S. & Medrano H. (2006b) Decreased Rubisco activity during water stress is not induced by decreased relative water content but related to conditions of low stomatal conductance and chloroplast CO2 concentration. *New Phytologist* **172,** 73–82.

Flexas J., Barón M., Bota J., Ducruet J.-M., Gallé A., Galmés J., ... Sajnani C. (2009) Photosynthesis limitations during water stress acclimation and recovery in the drought-adapted Vitis hybrid Richter-110 (*V. berlandieri* × *V. rupestris*). *Journal of Experimental Botany* **60,** 2361–2377.

Flexas J., Diaz-Espejo A., Gago J., Gallé A., Galmés J., Gulías J. & Medrano H. (2014) Photosynthetic limitations in Mediterranean plants: a review. *Environmental and Experimental Botany* **103,** 12–23.

Galle A., Florez-Sarasa I., Tomas M., Pou A., Medrano H., Ribas-Carbo M. & Flexas J. (2009) The role of mesophyll conductance during water stress and recovery in tobacco (*Nicotiana sylvestris*): acclimation or limitation? *Journal of Experimental Botany* **60,** 2379–2390.

Galle A., Florez-Sarasa I., El Aououad H. & Flexas J. (2011) The Mediterranean evergreen *Quercus ilex* and the semi-deciduous *Cistus albidus* differ in their leaf gas exchange regulation and acclimation to repeated drought and re-watering cycles. *Journal of Experimental Botany* **62,** 5207–5216.

Galmés J., Medrano H. & Flexas J. (2007) Photosynthetic limitations in response to water stress and recovery in Mediterranean plants with different growth forms. *New Phytologist* **175,** 81–93.

Grassi G. & Magnani F. (2005) Stomatal, mesophyll conductance and biochemical limitations to photosynthesis as affected by drought and leaf ontogeny in ash and oak trees. *Plant, Cell & Environment* **28,** 834–849.

Jones H. (1985) Partitioning stomatal and non-stomatal limitations to photosynthesis. *Plant, Cell & Environment* **8,** 95–104.

Keenan T., Sabate S. & Gracia C. (2010a) The importance of mesophyll conductance in regulating forest ecosystem productivity during drought periods. *Global Change Biology* **16,** 1019–1034.

Keenan T., Sabate S. & Gracia C. (2010b) Soil water stress and coupled photosynthesis–conductance models: bridging the gap between conflicting reports on the relative roles of stomatal, mesophyll conductance and biochemical limitations to photosynthesis. *Agricultural and Forest Meteorology* **150,** 443–453.

Limousin J., Misson L., Lavoir A.V., Martin N.K. & Rambal S. (2010) Do photosynthetic limitations of evergreen *Quercus ilex* leaves change with long-term increased drought severity? *Plant, Cell & Environment* **33,** 863–875.

Misson L., Limousin J., Rodriguez R. & Letts M.G. (2010) Leaf physiological responses to extreme droughts in Mediterranean *Quercus ilex* forest. *Plant, Cell & Environment* **33,** 1898–1910.

Niinemets U. (2007) Photosynthesis and resource distribution through plant canopies. *Plant, Cell & Environment* **30,** 1052–1071.

Perez-Martin A., Flexas J., Ribas-Carbó M., Bota J., Tomàs M., Infante J. & Diaz-Espejo A. (2009) Interactive effects of soil water deficit and air vapour pressure deficit on mesophyll conductance to CO2 in *Vitis vinifera* and *Olea europaea*. *Journal of Experimental Botany* **60,** 2391–2405.

Perez-Martin A., Michelazzo C., Torres-Ruiz J.M., Flexas J., Fernández J.E., Sebastiani L. & Diaz-Espejo A. (2014) Regulation of photosynthesis and stomatal and mesophyll conductance under water stress and recovery in olive trees: correlation with gene expression of carbonic anhydrase and aquaporins. *Journal of Experimental Botany* **65,** 3143–3156.

Sagardoy R., Vázquez S., Florez-Sarasa I., Albacete A., Ribas-Carbó M., Flexas J., . . . Morales F. (2010) Stomatal and mesophyll conductances to CO2 are the main limitations to photosynthesis in sugar beet (*Beta vulgaris*) plants grown with excess zinc. *New Phytologist* **187,** 145–158.

Tomás M., Flexas J., Copolovici L., Galmés J., Hallik L., Medrano H., . . . Niinemets Ü. (2013) Importance of leaf anatomy in determining mesophyll diffusion conductance to CO2 across species: quantitative limitations and scaling up by models. *Journal of Experimental Botany* **64,** 2269–2281.

Wilson K.B., Baldocchi D.D. & Hanson P.J. (2000) Quantifying stomatal and non-stomatal limitations to carbon assimilation resulting from leaf aging and drought in mature deciduous tree species. *Tree Physiology* **20,** 787–797.

Received 21 August 2014; received in revised form 16 September 2014; accepted for publication 23 September 2014

SUPPORTING INFORMATION

Additional Supporting Information may be found in the online version of this article at the publisher's web-site:

Note S1. Description of the photosynthesis model used in this study.

Note S2. Spreadsheet implementing the calculations described in this study.